Covellite CuS as a matrix for "invisible" gold: X-ray spectroscopic study of the chemical state of Cu and Au in synthetic minerals

Tagirov, B. R.; Trigub, A. L.; Kvashnina, K. O.; Shiryaev, A. A.; Chareev, D. A.; Nickolsky, M. S.; Abramova, V. D.; Kovalchuk, E. V.;

Originally published:

July 2016

Geochimica et Cosmochimica Acta 191(2016), 58-69

DOI: https://doi.org/10.1016/j.gca.2016.07.015

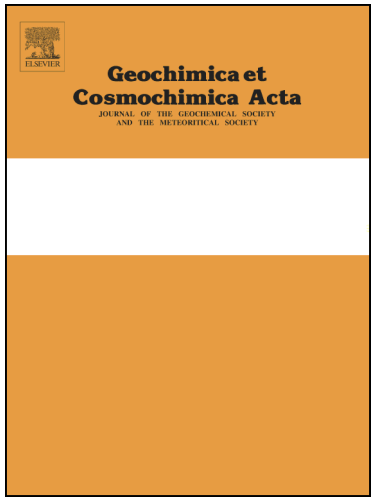

Covellite CuS as a matrix for "invisible" gold: X-ray spectroscopic study of the chemical state of Cu and Au in synthetic minerals

Boris R. Tagirov, Alexander L. Trigub, Kristina O. Kvashnina, Andrey A. Shiryaev, Dmitriy A. Chareev, Maximilian S. Nickolsky, Vera D. Abramova, Elena V. Kovalchuk

PII: S0016-7037(16)30395-7
DOI: http://dx.doi.org/10.1016/j.gca.2016.07.015
Reference: GCA 9850

To appear in: *Geochimica et Cosmochimica Acta*

Received Date: 23 August 2015
Accepted Date: 12 July 2016

Please cite this article as: Tagirov, B.R., Trigub, A.L., Kvashnina, K.O., Shiryaev, A.A., Chareev, D.A., Nickolsky, M.S., Abramova, V.D., Kovalchuk, E.V., Covellite CuS as a matrix for "invisible" gold: X-ray spectroscopic study of the chemical state of Cu and Au in synthetic minerals, *Geochimica et Cosmochimica Acta* (2016), doi: http://dx.doi.org/10.1016/j.gca.2016.07.015

Covellite CuS as a matrix for "invisible" gold: X-ray spectroscopic study of the chemical state of Cu and Au in synthetic minerals

Boris R. Tagirov[1]*, Alexander L. Trigub[2,7,1], Kristina O. Kvashnina[3,8], Andrey A. Shiryaev[4,1], Dmitriy A. Chareev[5,6,1], Maximilian S. Nickolsky[1], Vera D. Abramova[1] and Elena V. Kovalchuk[1]

[1] Institute of Geology of Ore Deposits (IGEM RAS), 35 Staromonetnyi per., 119017 Moscow, Russia

[2] National Research Centre 'Kurchatov Institute', 1 Akademika Kurchatova pl., 123182 Moscow, Russia

[3] ESRF, 38043 Grenoble, France

[4] Institute of Physical Chemistry and Electrochemistry (IPCE RAS), 31 korp. 4, Leninsky Prospect, 119071 Moscow, Russia

[5] Institute of Experimental Mineralogy (IEM RAS), 142432 Chernogolovka, Moscow Region, Russia

[6] Institute of Physics and Technology, Ural Federal University, Mira st., 19, 620002 Ekaterinburg, Russia

[7] Physico-Technical Institute of UB RAS, Kirova st. 132, 426000 Izhevsk, Russia

[8] Helmholtz-Zentrum Dresden-Rossendorf (HZDR), Institute of Resource Ecology, P.O. Box 510119, 01314, Dresden, Germany

*Corresponding author

Tel.: +7 (499) 230-82-31, Fax: +7 (495) 951-15-87, Email: tagir@igem.ru

Second revised version submitted to Geochimica et Cosmochimica Acta June 2016

ABSTRACT

Geological processes leading to formation of sulfide ores often result in precipitation of gold-bearing sulfides which can contain high concentrations of this metal in “invisible” (or ”refractory”) state. Covellite (CuS) is ubiquitous mineral in many types of the ore deposits, and numerous studies of the natural ores show that covellite can contain high concentrations of Au. At the same time, Au-bearing covellite withstands cooling in contrast to other minerals of the Cu-Fe-S system (chalcocite, bornite, chalcopyrite), where Au exsolves at low temperatures. This makes covellite a convenient model system for investigation of the chemical state (local environment and valence) of the “invisible” Au in copper-sulfide ores (copper-porphyry, epithermal, volcanogenic massive sulfide, SEDEX deposits). Therefore, it is necessary to determine the location of Au in the covellite matrix as it will have important implications for the methods employed by mineral processing industry to extract Au from sulfide ores. Here we investigate the chemical state of Cu and Au in synthetic covellite containing up to 0.3 wt.% of Au in the “invisible” state. The covellite crystals were synthesized by hydrothermal and salt flux methods. Formation of the chemically bound Au is indicated by strong dependence of the concentration of Au in covellite on the sulfur fugacity in the experimental system ($d(\log C(Au))/d(\log f(S_2)) \sim 0.65$). The Au concentration of covellite grows with increasing temperature from 400 to 450 °C, whereas further temperature increase to 500 °C has only minor effect. The synthesized minerals were studied using X-ray absorption fine structure spectroscopy (XAFS) in high energy resolution fluorescence detection (HERFD) mode. *Ab initio* simulations of Cu K edge XANES spectra show that the Cu oxidation state in two structural positions in covellite (tetrahedral and triangular coordination with S atoms) is identical: the total loss of electronic charge for the 3*d* shell is ~ 0.3 for both positions of Cu. This result is confirmed by theoretical analysis of electron density performed using quantum theory of atoms in molecules (QTAIM). Modeling of the Au L_3 edge EXAFS/XANES spectra showed that Au in covellite exists in the form of the

isomorphous solid solution formed by substitution for Cu atoms in triangular coordination with the Me-S distance in the first coordination shell increased by 0.18 Å relative to the pure CuS structure. The "formal" oxidation state of Au in covellite is +1. The Bader partial atomic charge for Au in covellite is lower than the charge of Cu (+0.2 e *vs.* +0.5 e) indicating that the degree of covalency for the Au-bearing covellite is higher than that of pure CuS. The analysis of electronic density of states shows that this structural position of Au results in strong interactions between hybridized Au *s,p,d*, S *p*, and Cu *p,d* orbitals. Such chemical bonding of Au to S and Cu can result in the formation of Au-bearing solid solution with other minerals in the Cu-Fe-S system.

1. INTRODUCTION

Gold is commonly associated with sulfide minerals in ores of magmatic, hydrothermal, and supergene origin. Pyrite (FeS_2), arsenopyrite (FeAsS), and Cu-Fe sulfides (chalcopyrite $CuFeS_2$ and bornite Cu_5FeS_4) are known to be the most important concentrators of Au in natural ores (see, for example, Genkin et al., 1999; Widler and Seward, 2002; Kesler et al., 2002; Bortnikov et al., 2003; Vikentyev et al., 2004, 2015, Wagner et al., 2007, Reich et al., 2010, Yudovskaya et al., 2015, and references therein). In these minerals Au exists mainly in the "invisible" (or "refractory") state. The "invisible" means that Au presents in the sulfide minerals as nanoscale particles and/or as isomorphous solid solution. Covellite (CuS), though not sufficiently abundant to account for significant part of Au resources, is present in most types of sulfide ores and is capable to incorporate the highest concentration of Au among minerals in the Cu-Fe-S system (Kesler et al., 2002). For high-sulfidation epithermal deposits it can be within the main hypogene ore mineral assemblage associated with Au mineralization (e.g. the world-class Zijinshan Cu–Au deposit, southeastern China, So et al., 1998; Wenyuan et al., 2016). Covellite possess an unusual layered structure (Fig. 1). The unit cell contains Cu atoms in tetrahedral and triangular coordinations (Cu_{Td} and Cu_{D3h}, respectively), whereas sulfur is present as single sulfide ions and disulfide S_2 groups (Evans and Konnert, 1976). In our recent study of synthetic covellites unusually high concentration - up to 0.3 wt.% - of homogeneously distributed "invisible" Au was observed (Tagirov et al., 2014). In contrast to all other sulfides in the Cu-Fe-S system covellite retains Au in the "invisible" state during quenching, whereas cooling of bornite and chalcopyrite results in exsolution of Au (c.f., Fraley and Frank, 2014) which makes covellite a convenient model system for investigation of the chemical state (local environment and valence) of the "invisible" Au.

The high content of Au in covellite can be explained by formation of isomorphous solid solution where Au either substitutes for Cu in the covellite lattice, or incorporates into the covellite matrix without distortions of the cationic sublattice. Therefore, in order to gain

insight into the nature of the solid solution between Au and Cu-Fe-S minerals, the chemical and oxidation states of both Cu and Au should be investigated. In the present study we employ X-ray absorption fine structure spectroscopy (XAFS) measurements in high energy resolution fluorescence detection (HERFD) mode (Glatzel and Bergmann, 2005) in order to reveal the chemical state of Cu and Au in synthetic covellites. For copper X-ray emission spectroscopy (XES) was also used in order to characterize filled electron orbitals. Interpretation of the spectra was performed using quantum chemical modeling and self-consistent X-rays absorption calculations.

2. EXPERIMENTAL METHODS

2.1. Synthesis of covellite and analytical methods

Hydrothermal (400 – 475 °C) and salt flux (495 °C) methods were used to synthesize covellite in Au-saturated system, i.e. in the presence of Au metal. In these experiments hydrothermal solution or 2 and 3-component eutectic mixtures of chlorides (liquid at the synthesis temperature) acted as a transport media and promoted attainment of chemical equilibrium. Chemical composition of the synthesized minerals was determined using three independent analytical techniques: electron microprobe (EPMA), laser ablation inductively coupled mass spectrometry (LA-ICP-MS), and wet chemistry. Details of the synthesis methods and of the analytical techniques are given in Supplementary EA1. SEM images of the synthesized minerals are shown in Fig. 2.

2.2. Spectroscopic measurements

The measurements were performed at beamline ID26 (Gauthier et al., 1999) of the European Synchrotron Radiation Facility (ESRF) in Grenoble. The incident energy was selected using the <111> reflection from a double Si crystal monochromator. Rejection of

higher harmonics was achieved by three Cr/Pd mirrors positioned at an angle of 2.5 mrad relative to the incident beam. The incident X-ray beam had a flux of approximately $2 \cdot 10^{13}$ photons s^{-1} on the sample position. XANES spectra were simultaneously measured in total fluorescence yield (TFY) mode using a photodiode and in high energy resolution fluorescence detection (HERFD) mode using an X-ray emission spectrometer (Glatzel and Bergmann, 2005; Kvashnina and Scheinost, 2016). The sample, analyzer crystal and photon detector (silicon drift diode) were arranged in a vertical Rowland geometry. The Cu HERFD spectra at the K edge were obtained by recording the maximum intensity of the Cu Kβ_1 emission line (8905.3 eV) as a function of the incident energy. The emission energy was selected using the <800> reflection of two spherically bent Ge crystal analyzers (1m curvature radius) aligned at 80° Bragg angle. A combined (incident convoluted with emitted) energy resolution of 0.9 eV was determined by measuring full width at half maximum (FWHM) of the elastic peak. The Au XANES/EXAFS HERFD spectra at the L_3 edge were obtained by recording the intensity of the Au Lα_1 emission line (9713 eV) as a function of the incident energy. The emission energy was selected using the <660> reflection of spherically bent four Ge crystal analysers (1m curvature radius) aligned at 80° Bragg angle. A combined (incident convoluted with emitted) energy resolution of 1.2 eV was determined by measuring the elastic peak. The intensity was normalized to the incident flux.

3. DATA TREATMENT

3.1. EXAFS data analysis

The EXAFS data ($\chi_{exp}(k)$) were analyzed using the IFEFFIT data analysis package (Ravel and Newville, 2005). EXAFS data reduction employs standard procedures for the pre-edge subtraction and spline background removal. Fourier transform (FT) of the k^2-weighted EXAFS function $\chi_{exp}(k)$ was calculated over the ranges of photoelectron wavenumbers k =

3.0–11.0 $Å^{-1}$. The photoelectron mean free path $\lambda(k)$, amplitude $F_i(k)$, and phase shift $\Psi_i(k)$ were calculated using program FEFF6 (Zabinskiy, 1995).

3.2. Density functional theory (DFT) calculations

Quantum chemical calculations were performed using DFT in the gradient-corrected approximation with an additional Hubbard-like term (GGA+U). The projector-augmented wave (PAW) all-electron description of the electron-ion-core interactions (Kresse, 1999), and the Perdew-Burke-Ernzerhof (PBE) exchange-correlation functional were used as implemented in QUANTUM ESPRESSO software package (Giannozzi et al., 2009). For the electronic structure calculations the self-consistent field (SCF) method was applied with 50 Ry kinetic energy cutoff for the plane waves, 700 Ry charge density cutoff, and SCF tolerance better than 10^{-8}. The system energy was calculated at a gamma point in a large 3×3×1 supercell which contained 108 atoms. The best parameter values for Hubbard corrections in covellite crystal (U = 5eV and J = 1eV) were accepted from Morales-García et al. (2014). The crystal structure optimization and optimization of supercell parameters were performed using the BFGS algorithm for atomic coordinates with convergence threshold 10^{-3} Ry/au for forces and 10^{-4} Ry for energy.

Topological charges were determined by means of the quantum theory of atoms in molecules (QTAIM, Bader, 1990, 1991). The analysis of topological charges in QTAIM starts from the determination of critical points of the electron density. Then the atomic basins are defined in accord with the determined critical points. The Bader charges are calculated by integrating the electronic density within the basins. Detailed topological analysis of the electron density for the covellite case is given in Morales-Garcia et al. (2014). In the present study the local atomic charges were calculated by integrating the charge density within Bader volumes around Cu, Au, and S atoms using CRITIC2 code (Otero-de-la-Roza et al., 2009; Otero-de-la-Roza et al., 2014).

3.3. XANES spectra modeling

Theoretical calculations of Cu K and Au L_3 edge spectra were performed using the FDMNES package (Joly, 2001; Guda, 2015). The Au L_3 edge spectra of Au-bearing covellites were simulated for the model structures optimized with the aid of QUANTUM ESPRESSO. Relativistic self-consistent field FDMNES calculations with the finite difference method (FDM) were used to solve the Schrödinger equation. The exchange-correlation part of the potential was used in a local density approximation following the Hedin and Lundqvist (1971) method. The final electronic states were calculated in a full core hole screening. Atomic clusters inside the spheres with radii of 7 Å were chosen for SCF calculations and for FDM XANES calculations of Cu K edge spectra and spectra of Au standards. Such cluster sizes were sufficient to accurately reproduce the main spectral features. For Au-bearing covellite the cluster sizes were fixed as 8 Å and 7 Å for SCF and FDM calculations, respectively. Despite the fact that this calculation procedure is computationally expensive, it represents the best choice for systems with non-spherical charge distribution. To account for many body effects and core hole lifetime broadening, the arctangent convolution was applied (Bunău and Joly, 2009). The crystal structure of Au_2S was accepted from Ishikawa et al. (1995), and the structure of covellite from Evans and Konnert (1976).

In addition to the Bader topological charges atomic charges calculated by FDMNES code (Bunău and Joly, 2009) are discussed.

4. RESULTS

4.1. The solubility of Au in covellite

Results of the solubility experiments are summarized in Table S1-1 (EA1) and plotted in Fig. 3a, b. In the hydrothermal experiments sulfur fugacity $f(S_{2(g)})$, calculated as described

in EA2, was buffered by elemental sulfur dissolution and hydrolysis reactions (Eqs. S3-1 – S3-4a, EA3). The $f(S_{2(g)})$ value in the salt flux experiments was close to that in equilibrium with liquid S. Effect of sulfur fugacity on the concentration (solubility) of Au in sulfide specifies the stoichiometry of the solubility reaction

$$Au_{(cr)} + n/2\ S_{2(g)} = AuS_{n(sulfide)} \quad (1)$$

and, therefore, the S/Au concentration ratio and the formal oxidation state of Au in the unit cell of the Au bearing sulfide. However, the true (not formal) structural position and the valence state of Au can only be determined by spectroscopic experiments described in the following section.

The concentration of Au in covellite reveals strong dependence on sulfur fugacity. The slope of the solubility curve vs. log $f(S_{2(g)})$ is equal to 0.65 ± 0.11 (Fig. 3a). This means that Au in the sulfide is chemically bound to sulfur and the S/Au concentration ratio in the hypothetical Au sulfide that forms solid solution with covellite is close to 0.65·2 = 1.3. The effect of temperature on the concentration of Au in covellite (Fig. 3b) indicates that ~0.3 wt.% represents the saturation limit: this concentration is attained at 450 °C, but further increase of temperature to 495 °C has negligible effect.

In order to calculate the concentration of "invisible" Au in covellite at low temperatures we assume that the equilibrium (1) constant linearly decreases as a function of 1/T(K) at $t \leq 450$ °C: $\log K_3 = -4825.7/T(K) + 4.48$ (for Au concentration expressed as mole fraction). Using this equation we can roughly estimate the maximum "invisible" Au content for covellite that coexists with $S_{(l)}$ and $Au_{(cr)}$ as: 10^{-7} ppm (120 °C), $5\cdot10^{-4}$ ppm (200 °C), $5\cdot10^{-2}$ ppm (250 °C), 1 ppm (300 °C), and 20 ppm (350 °C). For 400 °C the Au concentration in covellite in the S- and Au- saturated system is 450 ± 150 ppm, and for 450 - 500 °C temperature interval is 2400 ± 150 ppm (average values calculated using data from Table S1-1).

4.2. Au XAFS spectroscopy

4.2.1. Comparison with the reference substances

The Au L_3 edge HERFD-XANES spectrum of the Au-bearing covellite is compared to the reference substances in Fig.4 and Table 1. The HERFD spectra exhibit dramatic increase of the spectral features intensity compared to the TFY spectra. This makes possible proper assignment of the weak spectral features at low concentrations of admixtures (< 1 wt.% of Au in covellite). The L_3 edge absorption is related to the $2p$-$5d$ dipole-allowed transitions: $2p_{3/2} \rightarrow 5d_{5/2}/5d_{3/2}$. Therefore, the white line (WL) intensity reflects the number of empty states in $5d_{5/2}$ and $5d_{3/2}$ orbitals above the Fermi level.

The Au L_3 edge spectra for Au bearing covellite differs from the reference substances – metallic Au and Au_2S. The most important differences are: i) small WL (the feature A in Fig. 4) intensity for the covellite spectra which implies the lower unoccupied DOS for $5d$ orbitals; ii) the second feature (the feature B) in the covellite spectra is more intense than the feature A, whereas the reverse is true for the model substances, and iii) the position of the feature B is different: it is located at considerably lower energies in the case of covellite. Therefore, the chemical state of Au in covellite is neither metallic Au nor Au_2S. The Au^{3+} oxidation state is also ruled out due to marked dissimilarities in the position and intensity of the main features of Au in covellite and $HAuCl_4$.

4.2.2. Au L_3 edge EXAFS spectra analysis

Au L_3 edge EXAFS spectrum was used to probe the local atomic environment of Au in covellite. Results of EXAFS spectra fitting for Au_2S used as a model system are shown in Table S4-1 and Fig. S4-1 (EA4). Three structural models were used to retrieve initial atomic coordinates for the EXAFS spectra modeling: i) Au replaces Cu_{D3h}, ii) Au replaces Cu_{Td}, or iii) Au is incorporated inside the disulfide group with the formation of S-Au-S linear

structure. Good agreement between the experimental data and the model spectrum was achieved only for the Au in Cu_{D3h} position (Fig. 5a, b). The structural parameters refined from the spectrum fitting are listed in Table 2. The first coordination shell of Au is composed by 3 S atoms at a distance of 2.37 Å. Therefore, due to the difference in ionic radii, the Au-S distance increased by 0.18 Å compared to the Cu_{D3h}-S distance in pure covellite (last column in Table 2). For distant coordination shells comprising Cu and S atoms (Fig. 5b) the calculated values of Debye-Waller factor are quite large indicating significant distortion.

4.3. DFT calculations

At the first step of our DFT modeling crystallographic parameters of the covellite supercell $Cu_{72}S_{36}$ were optimized without constraints on symmetry. The calculated parameters of the relaxed supercell are compared to the tabulated crystallographic values in Table S5-1 (EA5); relative difference between the calculated and literature data is less than 1% for *a* and *b*, whereas *c* parameter is overestimated by 0.181 Å. The discrepancy can be caused by insufficient accuracy of the Γ-point approximation. To improve the agreement between the calculated structure and the experimental reference data more *k* – points should be used in the energy calculation (Morales-García et al., 2014). However, the level of theory used in our study is accurate enough to reproduce the main features of the experimental XANES spectra, as well as the bond lengths in pure covellite (Table 2).

The second step consisted in DFT simulations of three model systems with different positions of Au in covellite: i) Au substitutes for Cu_{Td} atom with the formation of $AuCu_{71}S_{36}$ supercell, ii) Au substitutes for Cu_{D3h} atom (supercell composition is equal to i), and iii) Au atom is placed between S atoms of the disulfide group with the formation of $AuCu_{72}S_{36}$ supercell. The crystallographic parameters of the modeled supercell were fixed in accord with the literature values (Table S5-1, first row), whereas individual atoms were allowed to relax. The calculated interatomic distances for modeled structures are listed in Table 2. Results of

Au L_3 edge EXAFS spectra analysis are in excellent agreement with the DFT calculation taking into account uncertainty of the EXAFS spectra modeling.

4.4. XANES spectra modeling

4.4.1. Cu in CuS

Experimental Cu K edge XANES/XES spectra of covellite are compared with the reference substances in Table S6-1 and Fig. S6-1a, b (EA4). The calculated spectra for Cu_{Td} and Cu_{D3h} are shown in Fig. 6. Both spectra exhibit obvious pre-edge feature at ~ 8979 eV. Its position is close to the E_F, and intensity reflects the unoccupied DOS (number of empty states) in the Cu hybridized 3*d*-4*p* shell (Fig. 7 and 8, see also discussion in Aquilanti et al., 2011). The similar pre-edge feature intensities imply close values of empty states in this shell and, therefore, similar oxidation state for both Cu_{Td} and Cu_{D3h} sites.

In contrast to the pre-edge position, intensities of the edge positions for the Cu_{Td} and Cu_{D3h} sites differ (Fig. 6) due to different geometries of the Cu local atomic environment. Analysis of the density of empty electronic states for the Cu_{D3h} atom (Fig. 8b) shows that shoulder at ~8982.3 eV (feature a, Fig. S6-1, Table S6-1) corresponds to transition from 1*s* to $4p_z$ states which are perpendicular to the triangle plane. This splitting of 4*p* states (and, therefore, of the Cu DOS peak) is absent for Cu_{Td} because of the local symmetry. At the same time, the WL (feature A) is attributed mostly to the interaction of Cu *p* and S *p* orbitals at the Cu_{Td} site (Fig. 7 b and d).

4.4.2. Au in CuS

The calculated spectra for the reference substances $Au_{(cr)}$ and $Au_2S_{(cr)}$ are compared to the experiment in Fig. S7-1 (EA7, an example of input files used for the FDMNES calculations is given in EA8). Good agreement of the calculated and experimental spectra makes possible accurate modeling of the XANES spectrum of Au-bearing covellite. Figure 9

compares calculated and experimental Au L_3 HERFD-XANES spectra for the "invisible" Au in covellite. In these calculations the spectra were generated for Au atoms incorporated into different positions in the covellite structure. Both Au in Cu_{Td} position and S-Au-S structure (when Au is incorporated inside the S_2 group separating the Cu_{Td} layers, Fig. 1) result in poor agreement with the experiment. The best agreement between the experimental and calculated spectra is observed when Au is placed in the Cu_{D3h} position.

4.5. Electronic structure

Results of the electronic structure calculations obtained using FDMNES code are shown in Fig. 7 and 8 (for Cu) and Fig. 10 (for Au). Bader atomic partial charges calculated using QTAIM are given in Table 3.

4.5.1. CuS

The calculated Cu 3*d* DOS integral (FDMNES code) at the Fermi level (E_F = 8978.5 eV) is 9.66 for the tetrahedral site and 9.73 for the triangular one. The DOS integral values of 4*s* and 4*p* states for both Cu_{Td} and Cu_{D3h} are also close to each other (Cu_{Td}: 4*s* = 0.41, 4*p* = 0.39; Cu_{D3h}: 4*s* = 0.38, 4*p* = 0.38). The sum of the *s*, *p*, and *d* electronic populations yields 10.46 for Cu_{Td} (the net charge +0.54) and 10.49 for Cu_{D3h} (the net charge +0.51). This implies that the valence state of Cu is almost equal for both sites. The equivalence of the atomic charges for Cu_{Td} and Cu_{D3h} sites is confirmed by the QTAIM analysis (Table 3) which is in close agreement with the FDMNES DOS calculation.

In addition to atomic charges calculated by means of quantum chemical methods, the "formal" oxidation state (atomic valence) of Cu in covellite can be estimated by the bond valence model (e.g. Brown, 1978, 2009). There are two positions of S atoms in the structure of covellite (Fig. 1): i) S1 atoms (single sulfide ions S^{2-}, position 2c) center trigonal bipyramids 3Cu1+2Cu2, and ii) S2 atoms (position 4e) form disulfide groups $[S_2]^{2-}$ that center

trigonal antiprisms 6Cu2. Assuming Pauling second rule one can see that each Cu atom receives 2/5 valence units (v.u.) from S1 atoms. The Cu1 atoms center triangles 3S1 and thus the charge of Cu1 is 3·(2/5)=1.2 v.u. The disulfide group $[S_2]^{2-}$ provides 2/6 v.u. to each Cu2 atom. A coordination polyhedron of the Cu2 is a 3S2+S1 tetrahedron, thus the charge of the Cu2 atom is 3·(1/3)+2/5=1.4 v.u. Assuming the convex shape of the bond length-bond valence curve (see Fig. 8 in Brown, 2009) we can expect that the Cu1-S1 bond valence is larger than the Cu2-S1 bond valence because the Cu1-S1 bond length is smaller than the Cu2-S1 one. It means that Cu1 valence is bigger than 1.2 v.u. and Cu2 valence is smaller than 1.4 v.u. Accordingly, the mean valence of Cu in covellite is equal to 1.3 v.u., and both positions of Cu atoms are almost equivalent in terms of the oxidation state.

These data can be compared with recent studies of the oxidation states of Cu and S in covellite. Based on DFT calculations Mazin (2012) showed that the appropriate ionic model for CuS is $(Cu^{4/3})_3(S_2^{2-})(S^{2-})$ with Cu valency 1.33 for both tetrahedral and triangular sites. Kumar et al. (2013) measured XAS/XES spectra for low-chalcocite Cu_2S and covelite and showed that Cu 3*d* empty states are present in both Cu_2S and CuS. These data are consistent with results of our Cu K edge XANES measurements (EA6): spectra of both $Cu_{2-x}S$ and CuS exhibit pre-edge feature, demonstrating presence of Cu 3*d* holes. Formally, the empty 3*d* states can be attributed to the presence of Cu^{2+}, but the real number of holes in 3*d* shell is < 1 as evaluated by quantum chemical calculations. Comparing spectroscopic data for various Cu sites geometries Kumar et al. (2013) concluded that $[(Cu_{Td})_2]^{3+}(Cu_{D3h})^{+}(S_2)^{2-}(S)^{2-}$ model (each Cu_{Td} site is $Cu^{+1.5}$) is more appropriate for the covellite electronic structure than a model where both Cu_{Td} and Cu_{D3h} sites formally possess Cu^{+2} centers. This conclusion, however, was not confirmed by quantum chemical calculations. Moralez-Garcia et al. (2014) used DFT method to calculate the covellite electronic structure followed by the QTAIM topological analysis of the electron density. Topological charges calculated by Moralez-Garcia et al. (2014) are close for Cu_{Td} and Cu_{D3h} sites: +0.44 e and +0.40 e, respectively, and are in good

agreement with data of Table 3. To summarise, all the above studies of the covellite electronic structure and the present work, are consistent with the presence of empty states in the Cu 3*d* shell both for the Cu_{Td} and Cu_{D3h} sites and the "formal" oxidation state of Cu is close to 1.3.

4.5.2. Au in CuS

Theoretical FDMNES calculations allow to assign the features of Au L_3 edge XANES spectra to peaks of the DOS function (Fig. 10). The WL feature corresponds to transition from $2p_{3/2}$ to hybridized Au *s,p,d* and S *p* orbitals, which are responsible for the formation of σ chemical bond. The second distinct peak (feature B, Table 1) originates mostly from the mixing of Au *d* and Cu *p* empty valence states. Therefore, its position is sensitive to the second coordination shell geometry, which is represented by octahedra formed by Cu atoms.

The atomic charge on Au atom (+0.19 e) calculated with QTAIM theory is much smaller than the charge on Cu atoms in covellite (+0.5 e ÷ +0.56 e, Table 3). This implies that deviation of Au-S bond from the ideal ionic model is higher than that for Cu-S bond (the degree of covalency of Au-S bond is higher).

5. CONCLUSIONS

The Cu K edge HERFD-XANES spectra, Au L_3 edge HERFD-XANES/EXAFS spectra, and Cu Kβ XES spectra were recorded for Au-bearing synthetic covellites CuS. Comparison of the experimental spectroscopic data with theoretically calculated spectra reveals electronic structure and valence state of Cu and Au in covellite and provides information about the structural position of Au in this mineral. The valence of Cu in both tetrahedral and triangular sites of covellite is identical and the "formal" oxidation state of Cu can be accepted as +1.3. Gold can form solid solution with covellite in which the "invisible" Au concentration can be as high as 0.3 wt.%. Here Au substitutes for Cu in triangular

coordination with S atoms. According to EXAFS spectra analysis and DFT calculations the Me-S bond length in the first coordination shell increases from 2.19 Å for Cu in pure covellite to 2.37 Å for Au-S bond. The oxidation degree of Au in covellite is well below than the Cu charge: Bader partial charges of Au and Cu in covellite are +0.2 e and +0.5 e, respectively. In this form of the solid solution Au is stabilized by the formation of chemical bond with 3 S atoms in the first coordination shell and with 6 Cu atoms in the second. Such chemical bonding is responsible for high stability of the high temperature "invisible" form of Au in covellite which can withstand cooling. We expect that the chemically bound "invisible" form of Au in covellite will prevent its extraction by the cyanide leaching widely used for the Au ores processing. Results of the present study suggest that in other minerals of the Cu-Fe-S system (digenite, chalcopyrite, bornite) at high temperature Au also can form solid solution by substitution for Cu atoms.

ACKNOWLEDGEMENTS

Authors acknowledge the ESRF for the beamtime allocation under proposals ES-184 and ES-360. B.R.T. and K.O.K. thank Hugo Vittoux for outstanding technical support during the in-situ experiment with micro-furnace at ID26 beamline. We are grateful to Jacques Schott and Oleg Pokrovsky for organizing visit of E.A.K. to Toulouse, and to Philippe de Parseval, Sophie Gouy and Thierry Aigouy for EMRA and SEM measurements at GET. We thank A.V. Zotov for constructive discussions during the course of the experimental study and important comments on the manuscript text. Valuable comments and suggestions from four anonymous reviewers and AE are greatly appreciated. Financial support of this study was provided by the Russian Scientific Foundation (grant 14-17-00693 - investigation of the chemical state of Au, grant 15-19-10002 – investigation of the chemical state of Cu), and RFBR grant 16-05-00938-a – salt flux synthesis. One of the authors (D.A.Ch) was supported by Act 211 Government of the Russian Federation, agreement № 02.A03.21.0006. Quantum chemical calculations were carried out using high-performance computing resources of Federal center for collective usage at NRC "Kurchatov Institute", http://computing.kiae.ru/.

REFERENCES

Aquilanti G., Giorgetti M., Minicucci M., Papini G., Pellei M., Tegoni M., Trasatti A. and Santini C. (2011) A study on the coordinative versatility of new N,S-donor macrocyclic ligands: XAFS, and Cu^{2+} complexation thermodynamics in solution. *Dalton Trans.* **40,** 2764-2777.

Bader R.F.W. (1990) *Atoms in molecules: a quantum theory.* Oxford University Press: Oxford, U.K.

Bader R.F.W. (1991) A Quantum Theory of Molecular Structure and its Applications. *Chem. Rev.* **91,** 893–928.

Bortnikov N.S., Cabri L.J., Vikentiev I.V., Tagirov B.R., Mc Mahon G., Bogdanov Yu.A. and Stavrova O.O. (2003) Invisible gold in sulfides from seafloor massive sulfide edifices. *Geology of Ore Deposits* **45,** No. 3, 201-212.

Brown I.D. (1978) Bond valences—a simple structural model for inorganic chemistry. *Chem. Soc. Rev.* **7,** 359-376.

Brown I.D. (2009) Recent developments in the methods and applications of the bond valence model. *Chem. Rev.* **109,** 6858-6919.

Bunău O. and Joly Y. (2009) Self-consistent aspects of x-ray absorption calculations. *J. Phys.*: *Condens. Matter* **21**, 345501.

Degoli E., Cantele G., Luppi E., Magri R., Ninno D., Bisi O. and Ossicini S. (2004) Ab initio structural and electronic properties of hydrogenated silicon nanoclusters in the ground and excited state. *Phys. Rev. B* **69,** 155411.

Evans H.T. and Konnert J.A. (1976) Crystal structure refinement of covellite. *Am. Mineral.* **61,** 996 - 1000.

Fraley K. J. and Frank M. R. (2014) Gold solubilities in bornite, intermediate solid solution, and pyrrhotite at 500° to 700°C and 100 MPa. *Econ. Geol.* **109,** 407-418.

Gauthier C., Sole V.A., Signorato R., Goulon J. and Moguiline E. (1999) The ESRF beamline ID26: X-ray absorption on ultra dilute sample. *J. Synchrotron Rad.* **6**, 164-166.

Giannozzi P., Baroni S., Bonini N., Calandra M., Car R., Cavazzoni C., Ceresoli D., Chiarotti G.L., Cococcioni M., Dabo I., Dal Corso A., de Gironcoli S., Fabris S., Fratesi G., Gebauer R., Gerstmann U., Gougoussis C., Kokalj A., Lazzeri M., Martin-Samos L., Marzari N., Mauri F., Mazzarello R., Paolini S., Pasquarello A., Paulatto L., Sbraccia C., Scandolo S, Sclauzero G., Seitsonen A.P., Smogunov A., Umari P. and Wentzcovitch R.M. (2009) QUANTUM ESPRESSO: a modular and open-source software project for quantum simulations of materials. *J. Phys.*: *Condens. Matter* **21**, 395502.

Glatzel P. and Bergman U. (2005) High resolution 1s core hole X-ray spectroscopy in 3d transition metal complexes - electronic and structural information. *Coord. Chem. Rev.* **249,** 65-95.

Guda S.A., Guda A.A., Soldatov M.A., Lomachenko K.A., Bugaev A.L., Lamberti C., Gawelda W., Bressler C., Smolentsev G., Soldatov A.V., Joly Y. (2015) Optimized finite difference method for the full-potential XANES simulations: application to molecular adsorption geometries in MOFs and metal-ligand intersystem crossing transients. *J. Chem. Theory Comput.* **11**, 4512-4521.

Hedin L. and Lundqvist B. (1971) Explicit local exchange-correlation potentials. *J. Phys. C: Solid State Phys.* **4,** 2064–2083.

Ishikawa K., Isonga T., Wakita S. and Suzuki Y. (1995) Structure and electrical properties of Au_2S. *Solid State Ionics* **79,** 60-66.

Joly Y. (2001). X-ray absorption near-edge structure calculations beyond the muffin-tin approximation. *Phys. Rev. B* **63,** 125120-125129.

Kesler S.E., Chyssoulis S.L. and Simon G. (2002) Gold in porphyry copper deposits: its abundance and fate. *Ore Geol. Rev.* **21,** 103-124.

Kresse G. (1999). From ultrasoft pseudopotentials to the projector augmented-wave method. *Phys. Rev. B* **59,** 1758–1775.

Kumar P., Nagarajan R. and Sarangi R. (2013) Quantitative X-ray absorption and emission spectroscopies: electronic structure elucidation of Cu_2S and CuS. *J. Mater. Chem. C* **1**, 2448-2454.

Kvashnina K.O. and Scheinost A.C. (2016) A Johann-type X-ray emission spectrometer at the Rossendorf Beamline. *J. Synchrotron Radiat., accepted.*

Morales-García A., Soares A. L., Dos Santos E.C., de Abreu H.A. and Duarte H.A. (2014) First-principles calculations and electron density topological analysis of covellite (CuS). *J. Phys. Chem. A* **118,** 5823–5831.

Otero-de-la-Roza A., Blanco M.A., Martín Pendás A. and Luaña V. (2009) Critic: a new program for the topological analysis of solid-state electron densities. *Comp. Phys. Com.* **180**, 157–166.

Otero-de-la-Roza A., Johnson E.R. and Luaña V. (2014) Critic2: A program for real-space analysis of quantum chemical interactions in solids. *Comp. Phys. Com.* **185**, 1007–1018.

Ravel B. and Newville M. (2005) ATHENA, ARTEMIS, HEPHAESTUS: data analysis for X-ray absorption spectroscopy using IFEFFIT. *J. Synchrotron Radiat.* **12,** 537-541.

Reich M., Kesler S., Utsunomiya S., Palenik C.S., Chryssoulis S.L. and Ewing, R.C. (2005) Solubility of gold in arsenian pyrite. *Geochim. Cosmochim. Acta* **69,** 2781-2796.

So C.S., Zhang D.Q., Yun S.T. and Li D.X. (1998) Alteration-mineralization zoning and fluid inclusions of the high sulfidation epithermal Cu-Au mineralization at Zijinshan, Fujian province, China. *Econ. Geol.* **93,** 961-980.

Tagirov B.R., Dikov Yu.P., Buleev M.I., Koval'chuk E.V., Chareev D.A., Kokh M.A., Borisovskii S.E., Abramova V.D., Baranova N.N., Garas'ko M.I., Kovalenker V.A. and

Bortnikov N.S (2014) “Invisible” gold in covellite (CuS): synthesis and studies by EPMA, LA–ICP–MS, and XPS techniques. *Doklady Earth Sciences* **459,** Part 1, 1381–1386.

Vikentyev I.V., Yudovskaya M.A., Mokhov A.V., Kerzin A.L. and Tsepin A.I. (2004) Gold and PGE in massive sulfide ore of the Uzelginsk deposit, Southern Urals, Russia. *Can. Miner.* **42,** 651-665.

Vikentyev I.V. (2015) Invisible and microscopic gold in pyrite: methods and new data for massive sulfide ores of the Urals. *Geology of Ore Deposits* **57,** No. 4, 237-265.

Wagner T., Klemd R., Wenzel T. and Mattsson B. (2007) Gold upgrading in metamorphosed massive sulfide ore deposits: direct evidence from laser-ablation-inductively coupled plasma-mass spectrometry analysis of invisible gold. *Geology* **35,** 775-778.

Wenyuan L., Cook N.J., Ciobanu C.L., Yua L., Xiaoping Q., Yuchuan C. (2016) Mineralogy of tin-sulfides in the Zijinshan porphyry–epithermal system, Fujian Province, China. *Ore Geol. Rev.* **72,** 682–698.

Widler A.M. and Seward T.M. (2002) The adsorption of gold (I) hydrosulphide complexes by iron sulphide surfaces. *Geochim. Cosmochim. Acta* **66,** 383-402.

Yudovskaya M.A., Distler V.V., Prokofiev V.Yu. and Akinfiev N.N. (2015) Gold mineralization and orogenic metamorphism in the Lena Province of Siberia as assessed from Chertovo Koryto and Sukhoi Log deposits. *Geoscience Frontiers*, *accepted.*

Zabinski S.I., Rehr J.J., Ankudinov A. and Alber R.C. (1995) Multiple-scattering calculations of x-ray-absorption spectra. *Phys. Rev. B* **52**, 2995-3009.

FIGURE CAPTIONS

Figure 1. Structure of covellite CuS (crystallographic data adapted from Evans and Konnert, 1976).

Figure 2. Backscattered electron images of covellite samples synthesized using hydrothermal technique at 450 °C, 1 kbar (a) and using salt flux method at 495 (hot end)/455 °C (cold end) (b). Both samples contain 0.3 wt.% Au.

Figure 3. Concentration of Au in covellite. A) *vs.* logarithm of sulfur fugacity log $f(S_2)$ for 450 °C, 1 kbar (hydrothermal synthesis); b) *vs.* temperature. The $f(S_2)$ value was calculated as described in EA2.

Figure 4. The Au L_3 edge HERFD- and TFY-XANES spectra of Au-bearing covellite and model substances. Position of the features labeled for each phase are listed in Table 1.

Figure 5. The k^2-weighted EXAFS spectra of Au in covellite (salt flux synthesis, RbCl/LiCl eutectic mixture, 495 (hot end)/455 °C (cold end)). Thin lines show the experimental spectra, thick curves - calculated spectra. *Left panel*: background subtracted EXAFS spectra. *Right panel*: Fourier transform of the EXAFS spectra (uncorrected for phase shift). The feature labels show scattering paths from different atoms and correspond to Table 2.

Figure 6. The Cu K edge spectra of covellite - comparison of theoretical (FDMNES code, Cu in tetrahedral Cu_{Td}, triangular Cu_{D3h} sites and their linear combination) and experimental spectra.

Figure 7. Calculated (FDMNES) a) Cu *s*-, b) Cu *p*-, c) Cu *d*-, and d) S *s*-, *p*- angular momentum projected DOS for Cu_{Td} and S atoms in the covellite structure. The experimental Cu K edge HERFD-XANES spectra and Cu Kβ XES spectra are given for comparison (black lines, normalized absorption/intensity is in arbitrary units). The scale of the Cu Kβ XES spectra is corrected for -2.5 eV in comparison with the experimental scale shown in Fig. S6-1b (spectra is shifted leftward from the Fermi level) to match the XANES scale.

Figure 8. The same as in Fig. 7 but for Cu_{D3h}.

Figure 9. The Au L_3 edge HERFD-XANES spectra of Au-bearing covellite (hydrothermal synthesis) compared to theoretical FDMNES calculations for Au in different positions in the covellite structure. The feature resulted from the presence of traces of Au metal is indicated by arrow.

Figure 10. Calculated (FDMNES) a) Au *s*-, b) Au *p*-, c) Au *d*-, d) S *s*-, *p*-, and e) Cu *p*-, *d* angular momentum projected DOS for Au bearing covellite (Au substitutes for Cu_{D3h}). The

Au L_3 edge HERFD-XANES experimental spectrum is given for comparison (normalized absorption is in arbitrary units).

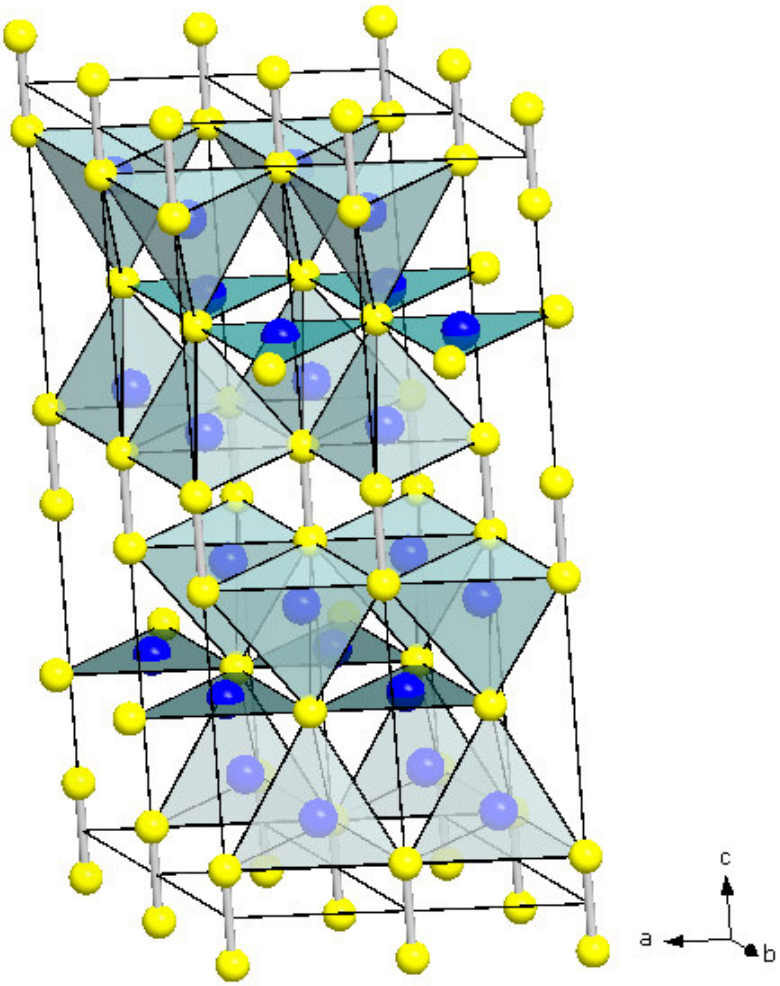

Fig. 1.

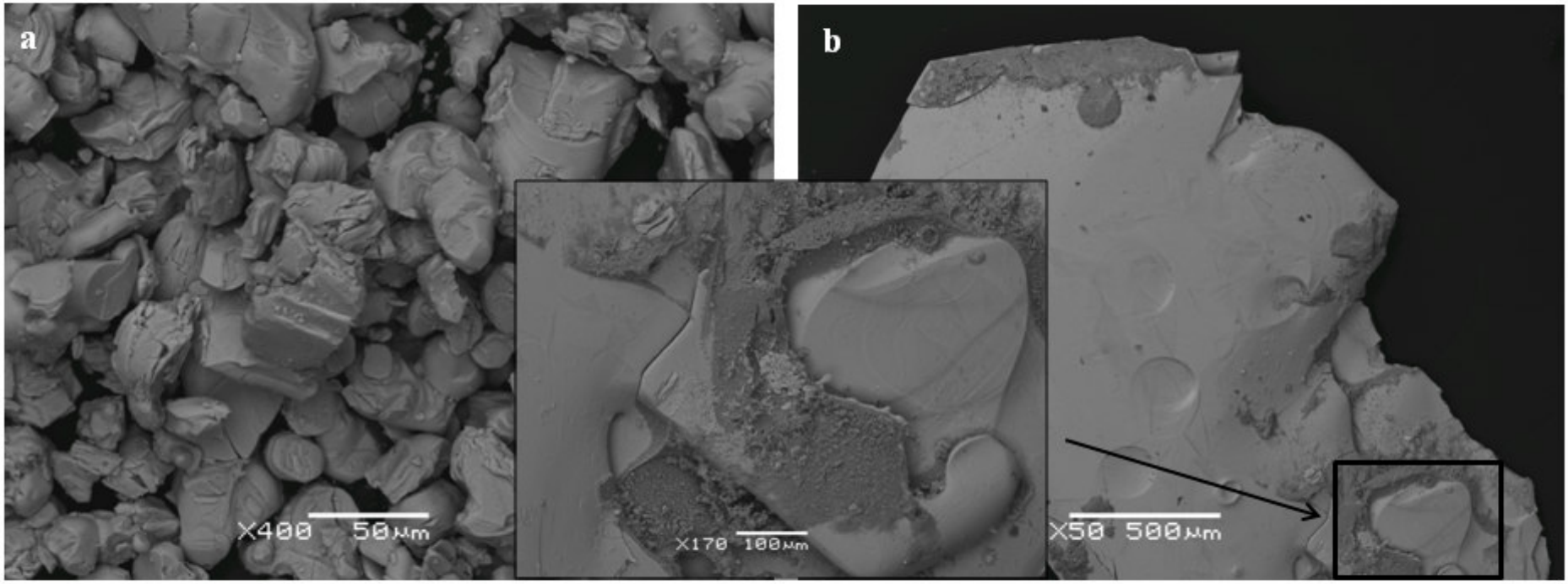

Fig. 2

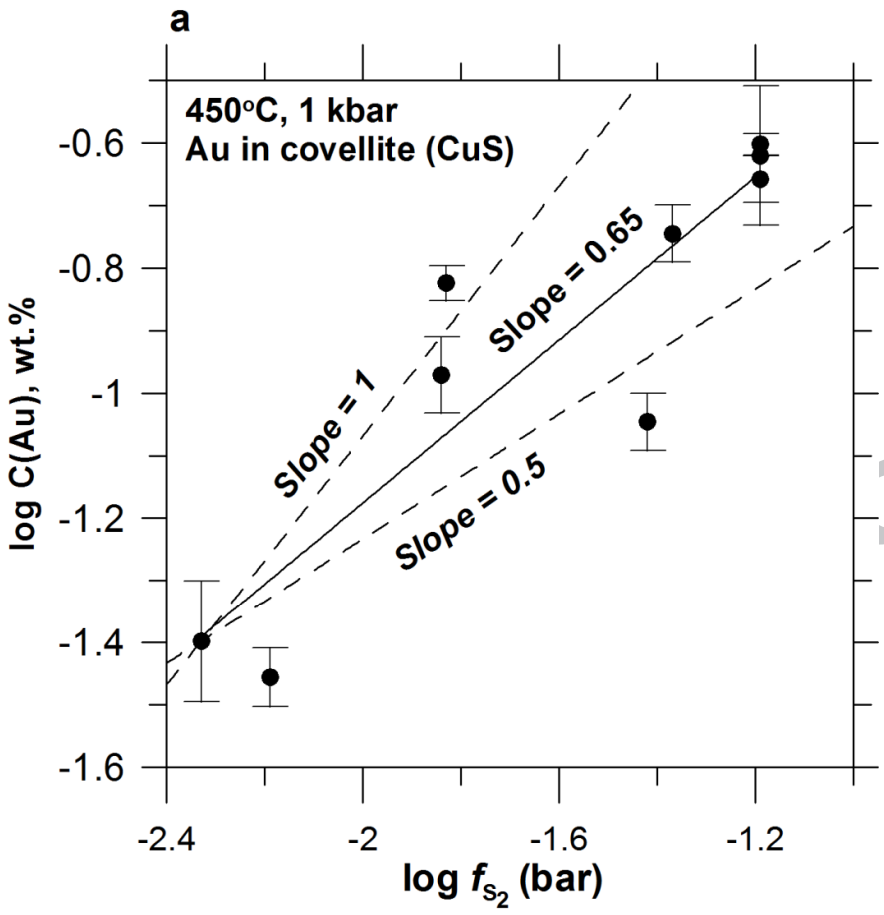

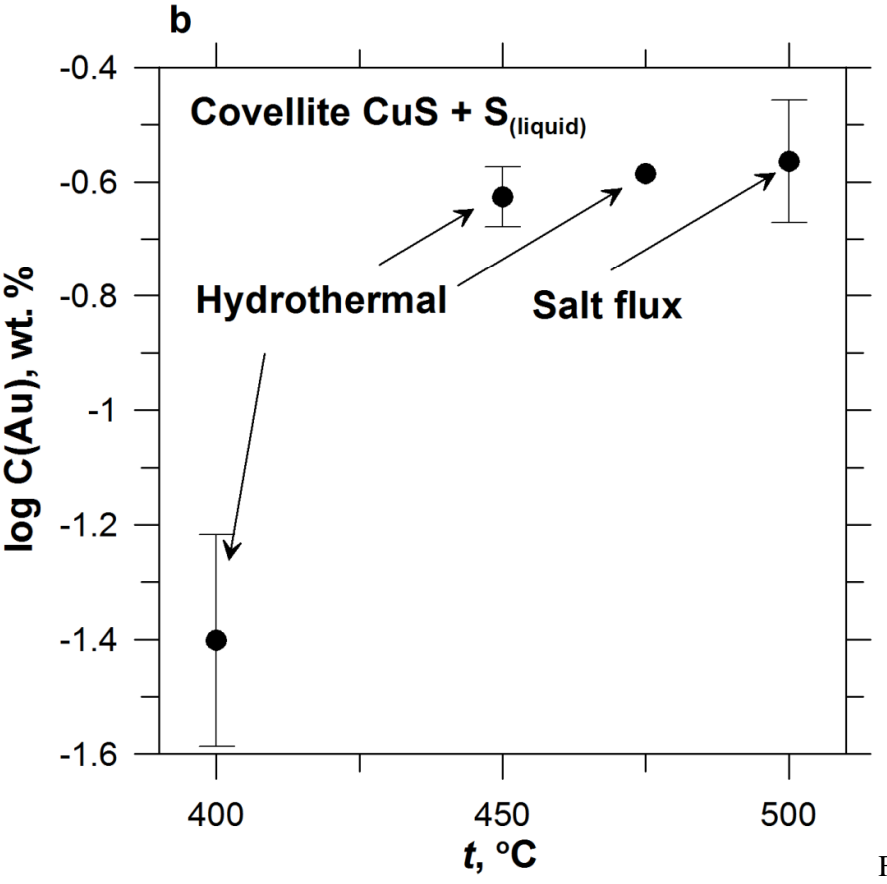

Fig. 3

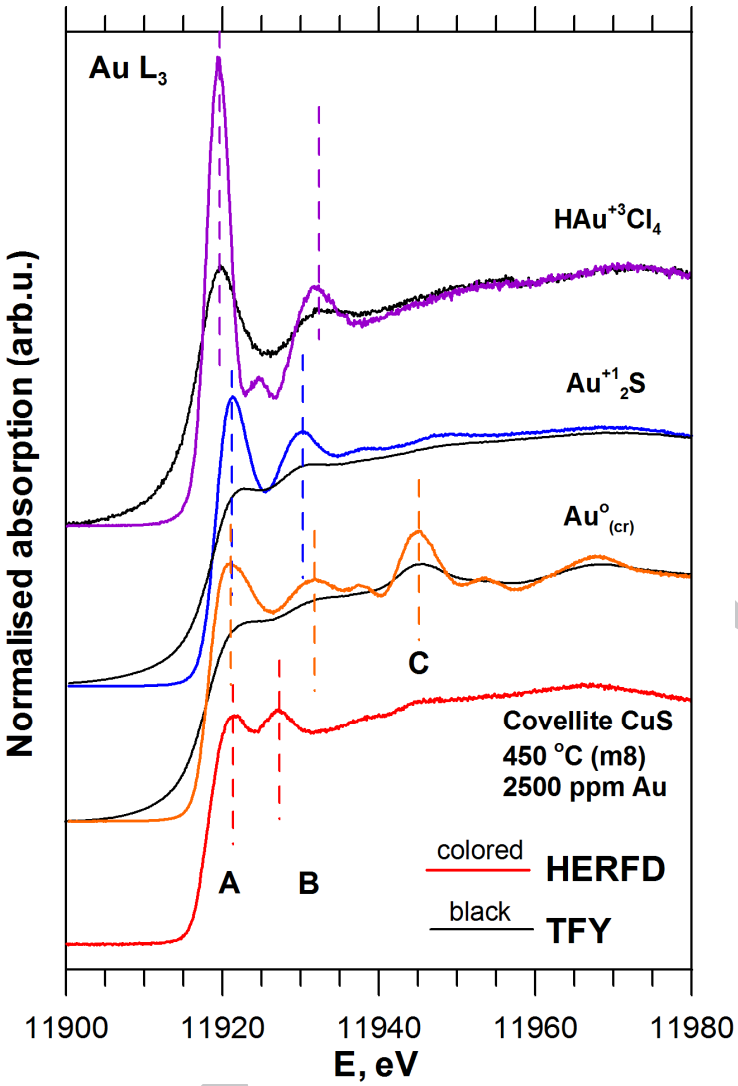

Fig. 4

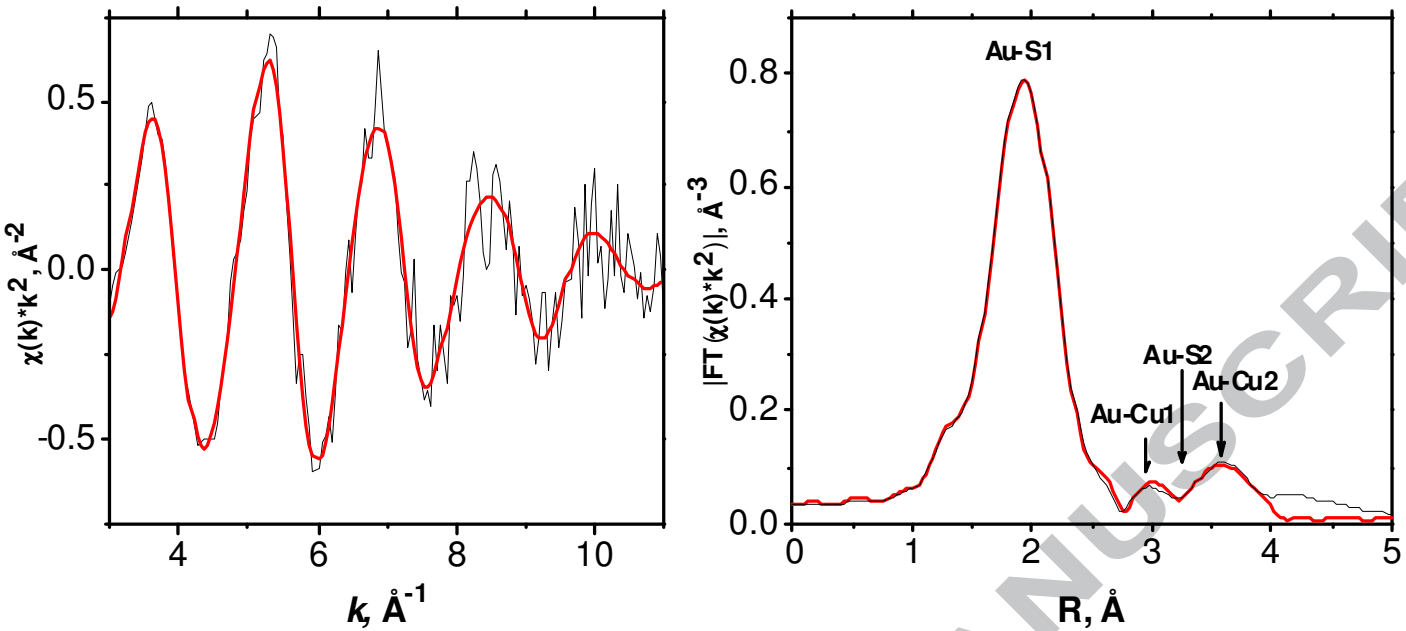

Fig. 5

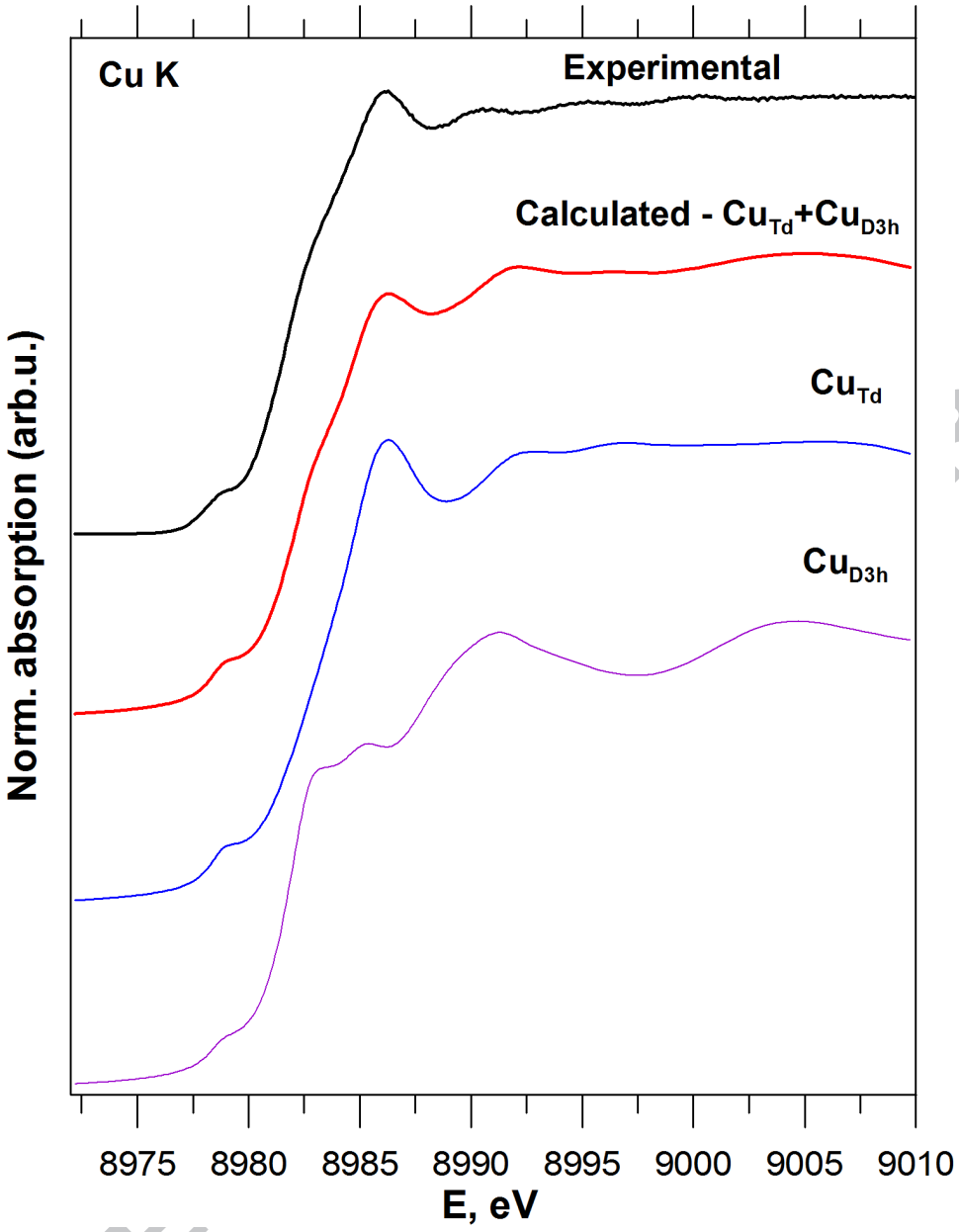

Fig. 6

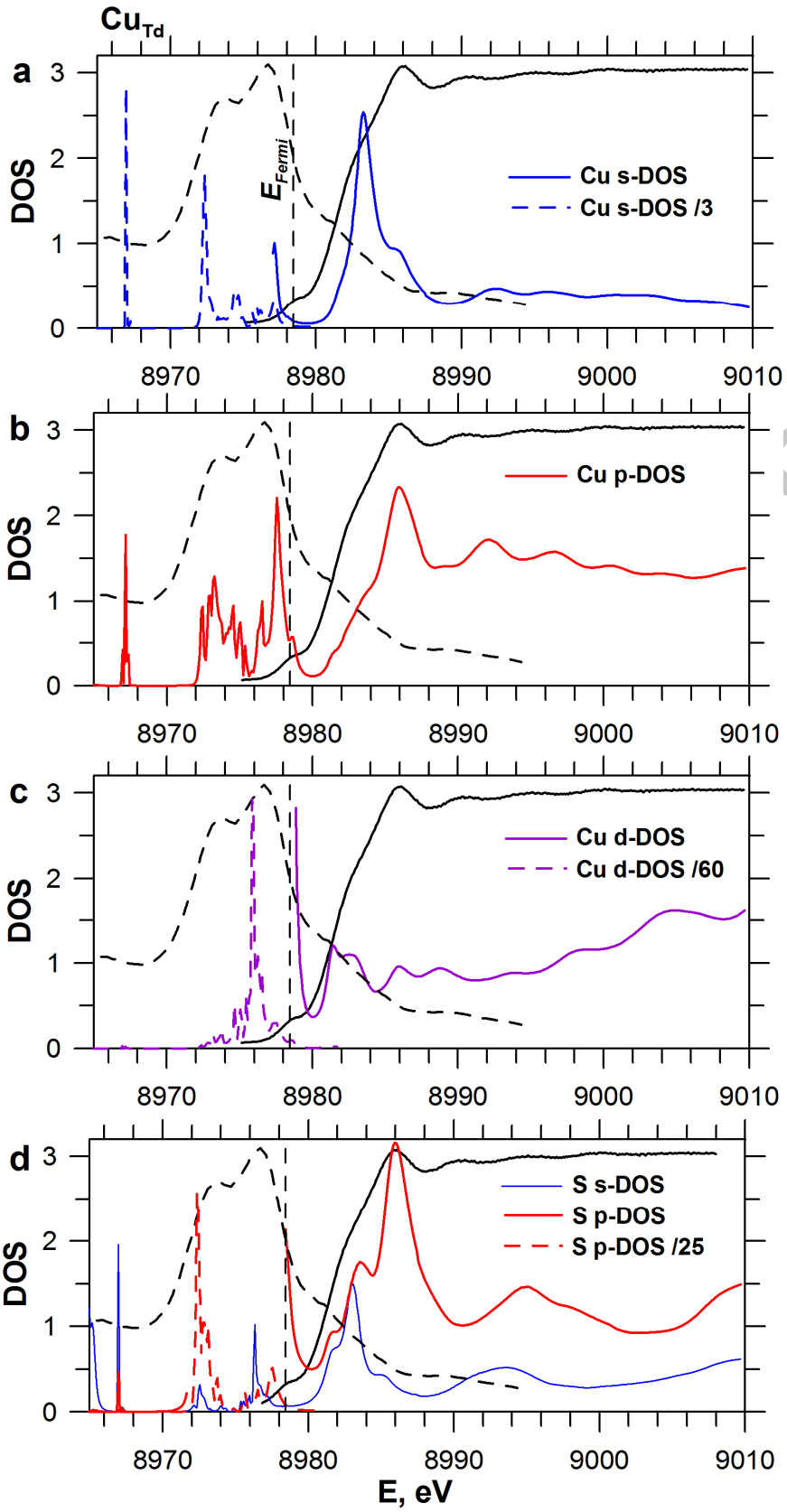

Fig. 7

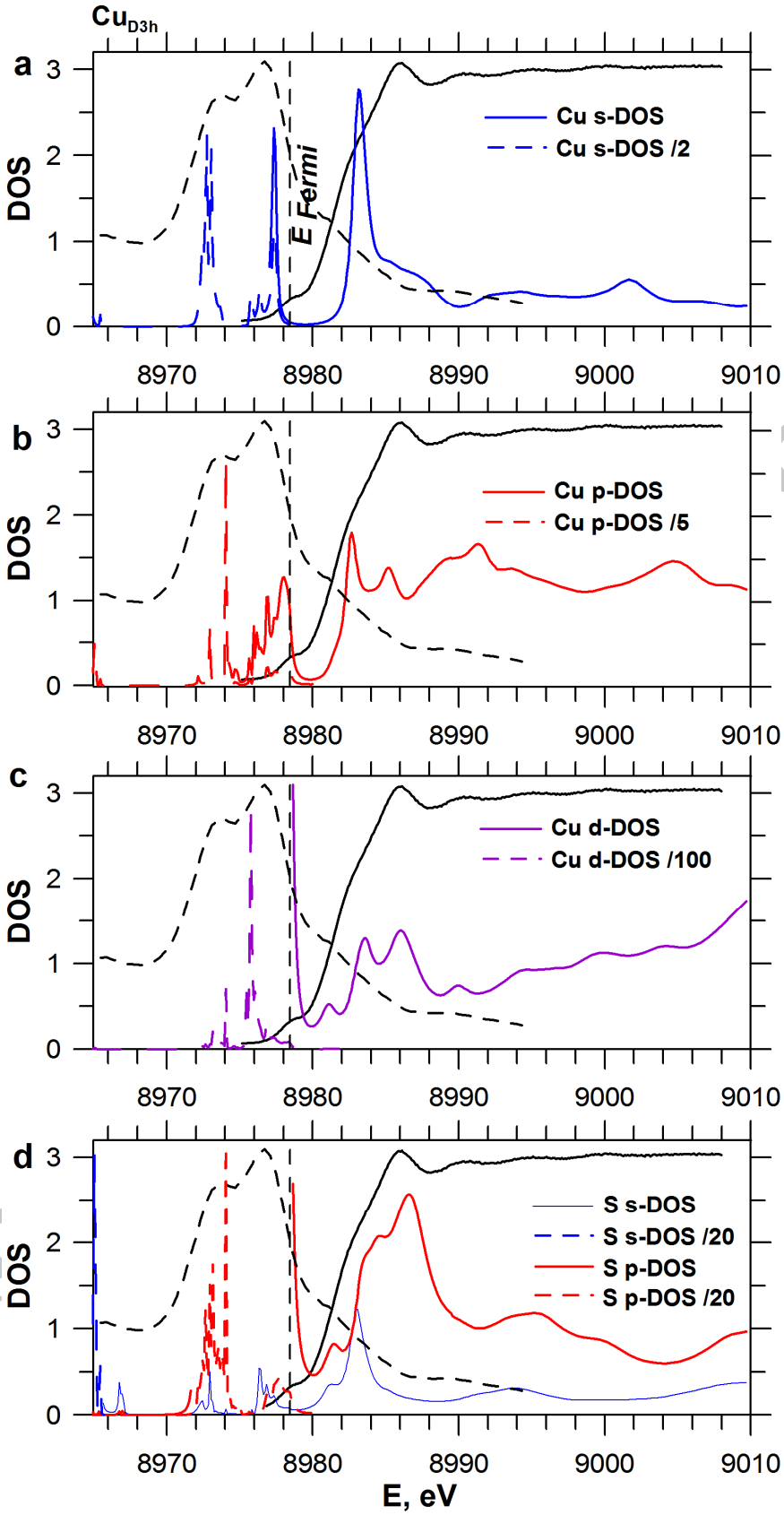

Fig. 8

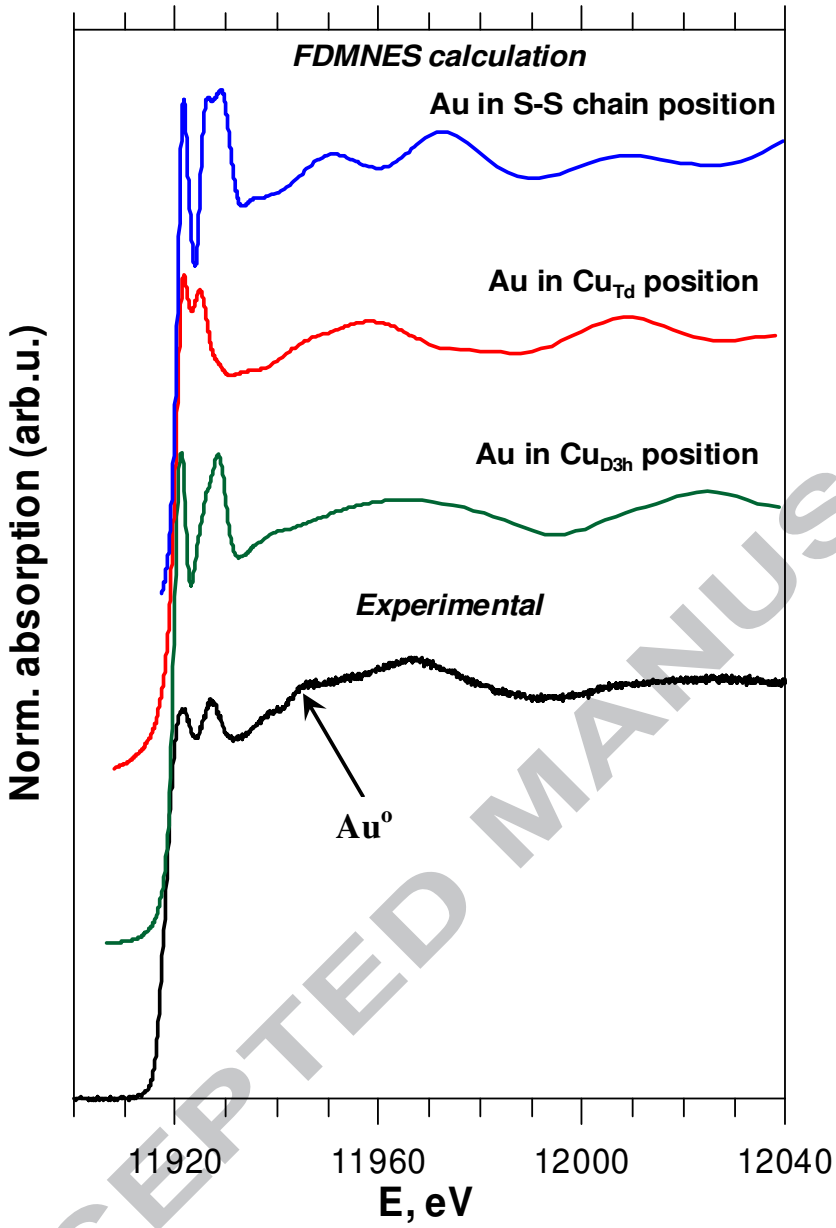

Fig. 9

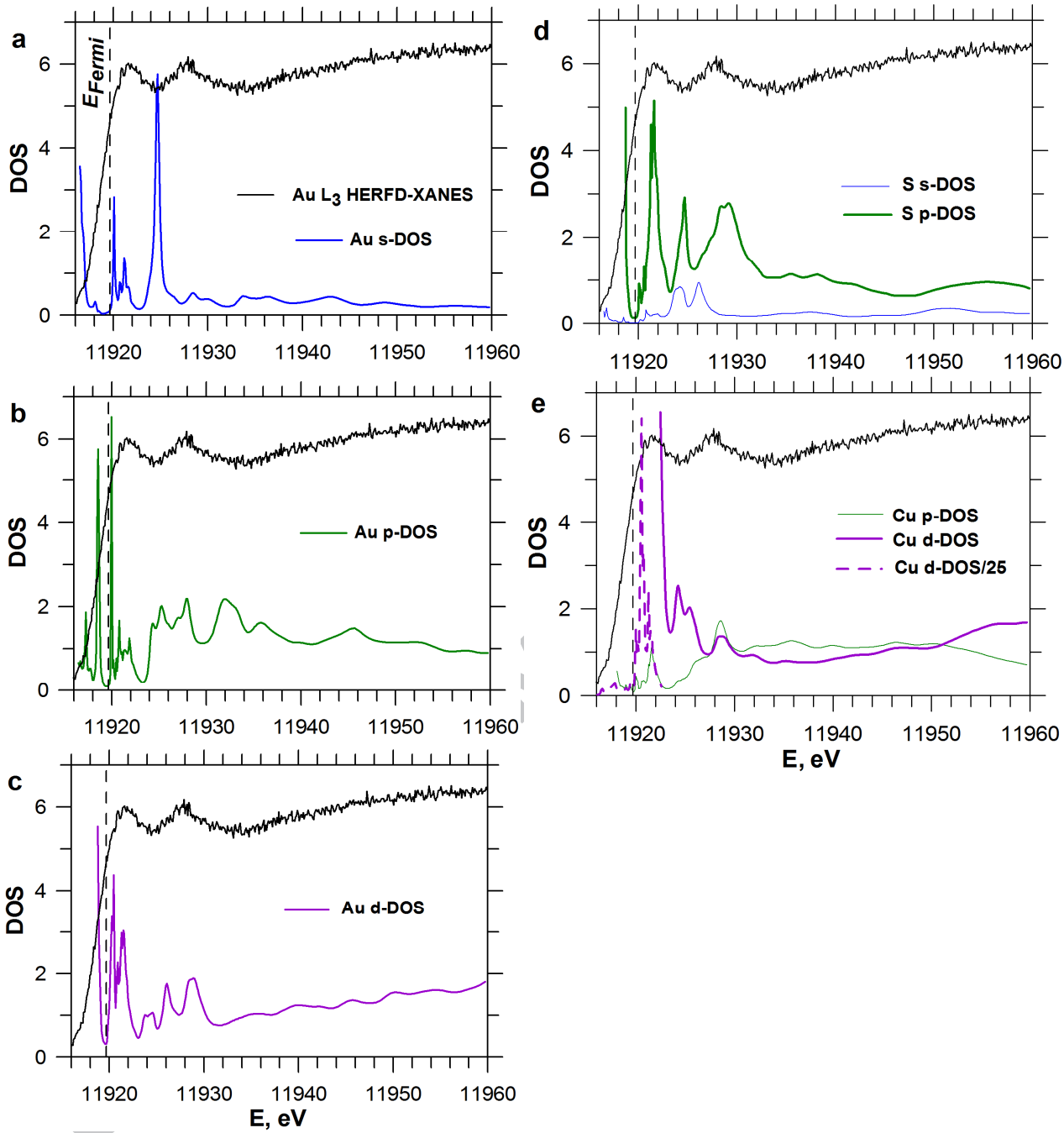

Fig. 10

Table 1. Position of edge jump (e.j.) and main features of Au L_3 edge HERFD-XANES spectra. Intense features are labelled by capital letters, weak features – by lower case letters. Uncertainty in the peak positions is ± 0.2 eV if not indicated otherwise.

Sample	Feature	Position, eV
Hydrothermal CuS 450 °C, 1 kbar 2500 ppm Au	e.j.	11918.2
	A	11921.5
	B	11927.2
	c	11938±1
	d	11946±1 (Au°)
	e	11967±1
$Au°_{(cr)}$	e.j.	11918.1
	A	11921.1
	B	11932.0
	c	11938±1
	d	11945.1
	d1	11953.6
$Au^{+1}{}_2S_{(cr)}$	e.j.	11919.0
	A	11921.3
	B	11930.2
	c	11938±1
	d	11948±1
$HAu^{+3}Cl_4{\cdot}4H_2O_{(cr)}$	e.j.	11917.6
	A	11919.5
	a	11924.7
	B	11931.7

Table 2. Au local atomic structure in covellite determined by EXAFS fitting and DFT calculations for Au atom in triangular, tetrahedral positions, and in linear position between S atoms. The last part of the table shows interatomic distances for unrelaxed covellite structure. Uncertainties are calculated by Artemis code.

Bond	Experimental					DFT optimization									Evans and Konnert (1976)		
	EXAFS (Au_{D3h})					Au_{D3h}		Au_{Td}		Au_{S2}		CuS, pure, Cu_{D3h}			Bond	Cu_{D3h}	
	N	*R*, Å	σ^2, Å^2	ΔE, eV	R-factor	*N*	*R*, Å	*N*	*R*, Å	*N*	*R*, Å	Bond	*N*	*R*, Å		*N*	*R*, Å
Au-S1	3.25 ±0.50	2.37 ±0.013	0.009 ±0.002	5.3±1.8	0.004	3	2.36	3 1	2.49 2.53	2	2.25	Cu-S1	3	2.21	Cu-S1	3	2.190
Au-Cu1	6	3.22 ±0.06	0.032 ±0.009			6	3.26	3	3.07	6	2.95	Cu-Cu1	6	3.24	Cu-Cu1	6	3.199
Au-S2	6	3.78 ±0.05	0.040 ±0.023			6	3.80	3	3.72	12	3.94	Cu-S2	6	3.80	Cu-S2	6	3.755
Au-Cu2	6	3.91 ±0.11	0.021 ±0.005			6	3.88	6	3.87	6	4.60	Cu-Cu2	6	3.83	Cu-Cu2	6	3.794

Table 3. Calculated Bader atomic partial charges for pure and Au-bearing covellite.

CuS	
Cu_{Td}	+0.56
Cu_{D3h}	+0.50
S	-0.84
S_2 group	-0.82
Au-bearing CuS (atoms closest to Au)	
Au_{D3h}	+0.19
S	-0.69
S_2 group	-0.80
Cu_{Td}	+0.56
Cu_{D3h}	+0.48